International Journal of Precision Engineering and Manufacturing (2023) 24:571–583
https://doi.org/10.1007/s12541-022-00752-w

Online ISSN 2005-4602
Print ISSN 2234-7593

REGULAR PAPER

Composite Layer Design Using Classical Laminate Theory for High Pressure Hydrogen Vessel (Type 4)

Gunyoung Park[1] · **Chul Kim**[2]

Received: 28 September 2022 / Revised: 23 November 2022 / Accepted: 24 November 2022 / Published online: 2 February 2023

Abstract
As air pollution becomes more severe, the use of clean energy in vehicles is an inevitable requirement and it is leading the development of automotive industries. Especially, hydrogen-fueled vehicles require safe and lightweight high pressure storage vessels to carry enough amounts of hydrogen gas. To develop mechanically robust and lightweight high pressure vessel, it is of significance to establish design and manufacturing process for liners and carbon fiber reinforced plastics layers. In this study, to design a composite layer in a high pressure hydrogen vessel (Type 4), a calculation method of stress generated in each ply by applying the CLT (Classical Laminate Theory) is proposed. And based on the calculation method, we carried out the composite layer design in the hydrogen high pressure vessel (Type 4) that can satisfy the requirement for lightweightness and designed the thickness and the pattern of the composite layer with more accuracy than the netting theory and with more rapid than FEA.

Keywords High pressure hydrogen vessel (Type 4) · CLT · Netting analysis · Composite layer

1 Introduction

The emissions from the use of fossil fuels have caused harmful substances, which threaten human health and the earth's environment, so there is an increase in the demand for clean and safe energy, and renewable energy needs to be used to achieve sustainable energy systems [1–5]. Especially in the public transport necessary for people's lives, a hydrogen storage pressure vessel is one of important devices for new energy vehicles. As the air pollution becomes more serious, safe and lightweight energy storage pressure vessel is inevitable requirements for development of the automotive industry [6–10]. A high pressure hydrogen vessel for vehicles is manufactured as Type 4 reinforcing a composite material on a plastic liner for light weight, and since the composite material supports most of the load by internal pressure, the design of a composite layer is the most important part in the high pressure hydrogen vessel (Type 4) [11, 12]. A composite layer of the hydrogen high pressure vessel (Type 4) is laminated through repeated arrangements of the helical winding for reinforcing a dome part and that of the hoop winding for reinforcing a cylinder part as shown in Fig. 1. In the previous studies relating to the high pressure hydrogen vessel using the composite material, Musthak developed the mathematical modelling for a pressure vessel with design pressure of 50 bar by using the netting analysis to originate variable thickness on entire structure [13]. Sapre deals with finite element modelling and analysis (FEM&A) to investigate mechanical/thermal stresses, strain, and deformation produced at the ply level of the tank, and the results of FEM&A are compared with published experimental results [14]. Cho studied the isotensoid dome design by carrying out a series of the hydraulic burst tests and the structural analyses for Type 4 composite cylinders [15].

Alcantar analyzed composite materials of the Type 4 pressure vessel with classical laminate theory and performed the FEA using the results obtained from vessel optimization [16]. Hua's research focused on reducing the composite weight with modelling assessment of conventional tanks without doilies that utilize lower cost resin that also has a low density, and of an alternate tank design [17]. Leh

✉ Chul Kim
chulki@pusan.ac.kr

[1] Research Institute of Mechanical Technology, Pusan National University, 2, Busandaehak-Ro 63Beon-Gil, Geumjeong-Gu, Busan 46241, Republic of Korea

[2] School of Mechanical Engineering, Pusan National University, 2, Busandaehak-Ro 63Beon-Gil, Geumjeong-Gu, Busan 46241, Republic of Korea

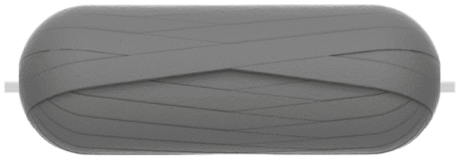

(a) Helical winding

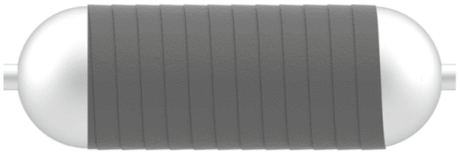

(b) Hoop winding

Fig. 1 Schematic of helical winding and hoop winding

presented and qualified an FE model taking into account progressive damage of the composite structure manufactured by filament winding and designed for a new optimization procedure developed specifically [18]. Jois analysed the effect of different dome geometries on the stress distribution at the dome cylinder interface [19]. Zhang presented methods for designing the lay-up and determining the range of internal pressure of the polymer liner based on the netting theory and FEA [20].

As described above, most previous studies on high pressure hydrogen vessels have been mainly focused on the design of the composite layer and the dome shape. The design of a composite layer is typically performed using the netting theory, one of the methods to calculate the thickness of composite layers. The netting theory cannot reflect changes in the laminate angle of each ply, and has limitations in terms of the accuracy of calculation results since multiple plies comprising a laminated structure are assumed to be a single ply. In addition, since continuously changing the thickness of the composite layer in the dome part cannot be calculated by the netting theory, there are some limitations in carrying out the design of the composite layer. To overcome these problems, design of the pattern and the thickness of the composite layer is generally performed using finite element analysis (FEA). However, compared to analyses assuming that the composite layer is composed of a single ply, a relatively longer time for an analysis is required since multiple plies are laminated, and since a number of design variables, including the laminate angle and pattern, need to be taken into account, design work also takes a considerable time. In order to overcome the limitations of the design using the netting theory and FEA mentioned above, the CLT (Classical Laminated Theory) can be used to calculate the stress generated in each ply. The high pressure hydrogen vessel (Type 4) consists of a dome part, a cylinder part, and a junction part connecting the dome part and the cylinder part. To calculate the stress of each ply in the high pressure hydrogen vessel (Type 4), both line loads (N_x, N_y) on the cylinder part and line moment (M_0) and line loads (N_x, N_y) in domes and junction parts should be considered. Because the line loads and the line moment in the dome parts are continuously changed at each point and the stress of each ply is quite difficult to calculate, there is lack of research about the high pressure hydrogen vessel (Type 4). And, because the dome parts of the high pressure hydrogen vessel (Type 4) is mainly designed as an isotensoid shape, a fracture of the composite layer occurs at the junction part except some cases having defects on a material. So, to design the high pressure hydrogen vessel (Type 4) using CLT, predicting the stress of each ply, which needs definition of the line moment (M_0) at the junction part, is very important and its configuration is shown in Fig. 2.

In this study, when the internal pressure is applied to the inner wall, the line loads (N_x, N_y) in the cylinder part and the line moment (M_0) in the junction part are to be defined, and the stress generated in each ply is calculated. Based on the above method, the thickness and pattern of the composite layer are designed with more accuracy than the netting theory and with more rapid than FEA.

2 Stress Calculation in Composite Layers Using CLT

2.1 Ply Axis Stress Calculation in a Cylinder Part of a High Pressure Hydrogen Vessel

When the internal pressure is applied to a high pressure hydrogen vessel (Type 4), the ply axis stress generated in a composite layer is obtained by consecutively calculating the stiffness matrix, the transformed stiffness matrix, the extensional stiffness matrix, laminate axis strain, laminate axis stress, and ply axis stress in the order presented here, as shown in Fig. 3 [21–23]. When internal pressure is applied to a pressure vessel, there is almost no effect of bending in the cylinder part, and thus a line load is generated in the longitudinal direction (N_x) and the hoop direction (N_y), as shown in Fig. 4. The line load applied to the laminated plate of the high pressure hydrogen vessel (Type 4) is obtained by Eq. (1). In Eq. (1), r_A is the distance from the central axis to the midpoint of the total thickness of the laminated composite layer of the pressure vessel as shown in Fig. 5.

$$\begin{cases} \mathrm{N_x} = \frac{\mathrm{Pr_A}}{2} \\ \mathrm{N_y} = \mathrm{Pr_A} \end{cases} \tag{1}$$

To calculate ply axis stress generated in the laminated plate of a high pressure hydrogen vessel (Type 4), it is necessary to identify the properties of a composite material, such as the

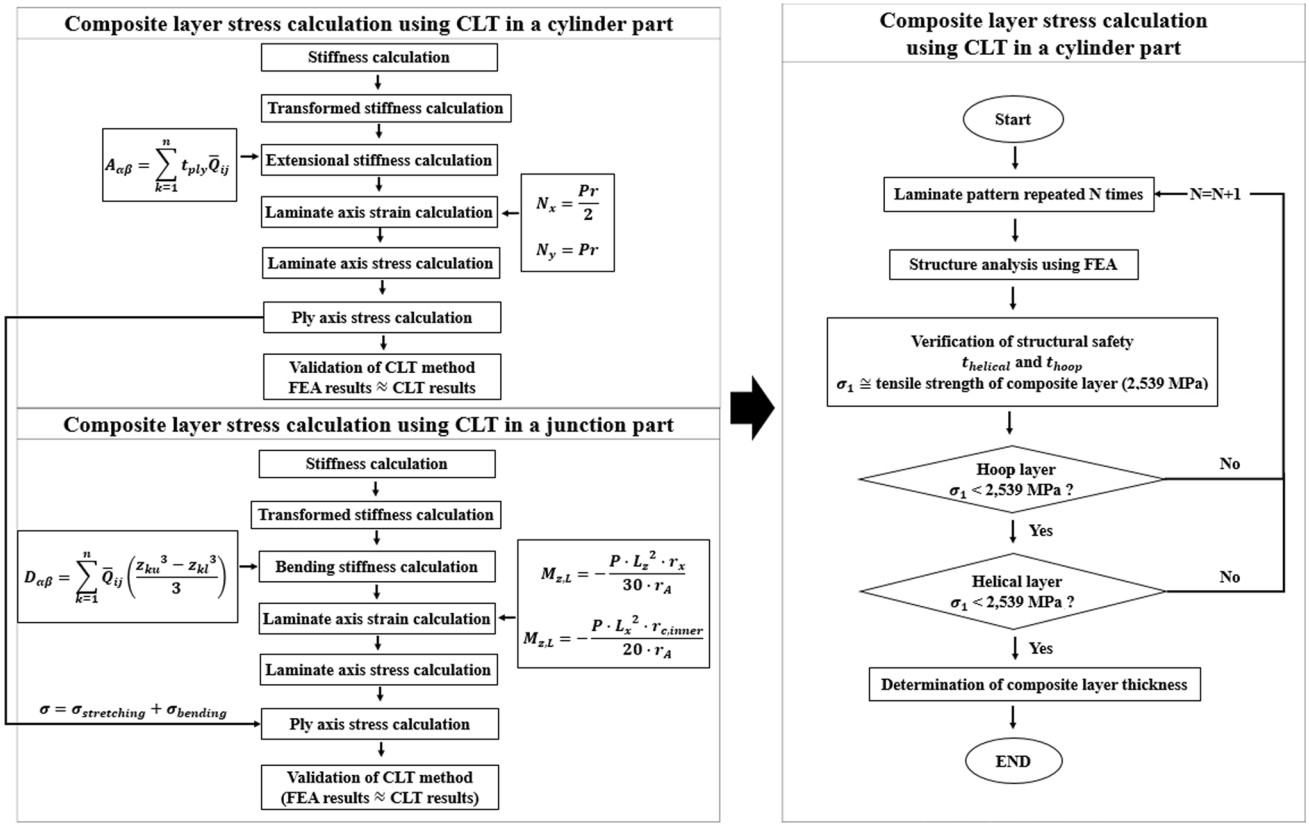

Fig. 2 Configuration of composite layer design for the high pressure hydrogen vessel (Type 4) using CLT

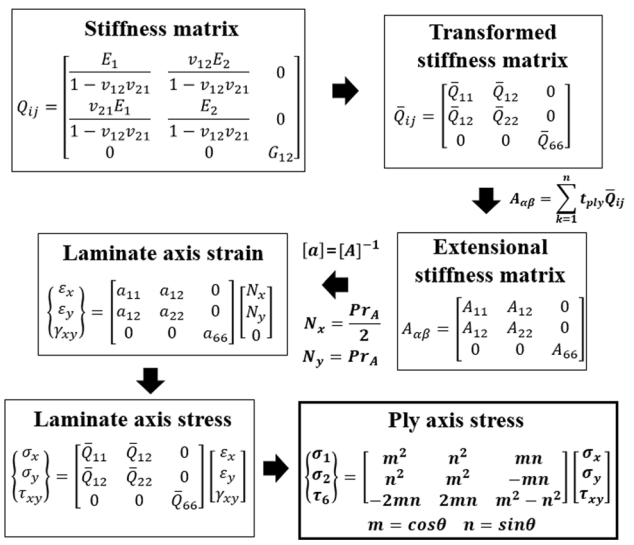

Fig. 3 The flow chart for calculation of ply axis stress of the high pressure hydrogen vessel (Type 4)

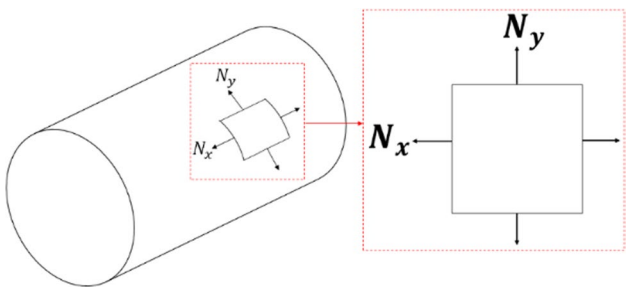

Fig. 4 Line loads generated in the cylinder part when internal pressure is applied

modulus of elasticity (E_1, E_2=E_3) and the poisson's ratio (ν_{23}, ν_{12}=ν_{13}), as shown in Table 1, the line loads generated in the composite layer when internal pressure is applied, and the thickness and laminate angle of the composite material. For the high pressure hydrogen vessel shown in Fig. 6, the thicknesses of the helical layer and hoop layer were calculated using the netting theory and the FEA, and they were determined to be 6 mm and 9.3 mm, respectively [24]. In this case, the laminate angle (α_c) in the cylinder part was calculated to be 11.54° by Eq. (2).

$$\alpha_c = \sin^{-1}\frac{r_o}{r_c} \tag{2}$$

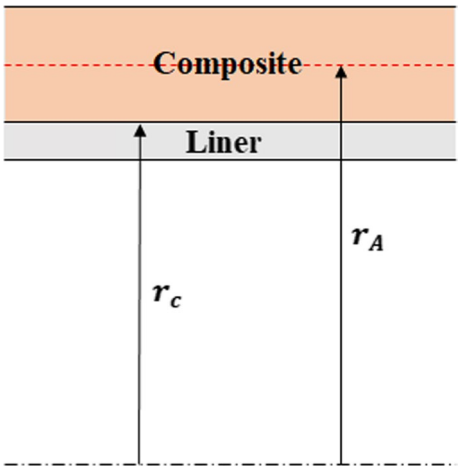

Fig. 5 Schematic of a cylinder part with a composite layer

Table 1 Dimension of a liner for a high pressure hydrogen vessel (Type 4) adopted in hydrogen automobiles

Property of composite (T700/Epoxy)		Design condition of composite	
E_1 (GPa)	137	P_{burst}	157.5 MPa
$E_2 = E_3$ (GPa)	9.1	α_c	11.54°
$\nu_{12} = \nu_{13}$	0.34	$t_{helcial}$	6 mm
ν_{23}	0.43	t_{hoop}	9.3 mm
$G_{12} = G_{13}$ (GPa)	4.71	r_c	150 mm
G_{23} (GPa)	3.1	N_x	12,414.9 N/mm
σ_f(MPa)	2539	N_y	24,830 N/mm

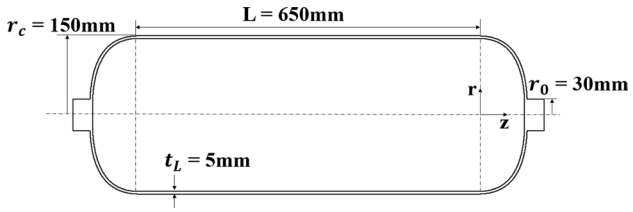

Fig. 6 Dimension of a liner for a high pressure hydrogen vessel (Type 4) adopted in hydrogen automobiles

Based on the conditions given in Table 1, in order to calculate ply axis stress for the high pressure hydrogen vessel (Type 4) in the order given in Fig. 3, the transformed stiffness matrix ($\overline{Q}_{ij}$) and the extensional stiffness matrix ($A_{\alpha\beta}$) were first calculated, respectively, as shown in Table 2. In this case, the total thickness of the composite layer in the cylinder part is 15.3 mm ($t_{helical}$: 6 mm and t_{hoop}: 9.3 mm). If the transformed stiffness matrix ($\overline{Q}_{ij}$) and the extensional stiffness matrix ($A_{\alpha\beta}$) are obtained, the laminate axis strain (ε_x) of each ply can be calculated, and the laminate axis stress (σ_x) can be determined. Finally, to assess structural safety for the fiber direction of the composite layer, ply axis transformation is required using the transformation matrix [J_1] as shown in Eq. (3), and ply axis stress (Maximum principal stress: σ_1) was calculated by Eqs. (4). The meanings of symbols in Eq. (3) are as follows: $m = \cos\theta$, $n = \sin\theta$.

$$\left[J_1\right] = \begin{bmatrix} m^2 & n^2 & 2mn \\ n^2 & m^2 & -mn \\ -mn & mn & m^2 - n^2 \end{bmatrix} \tag{3}$$

$$\begin{Bmatrix} \sigma_1 \\ \sigma_2 \\ \sigma_6 \end{Bmatrix} = \left[J_1\right] \begin{Bmatrix} \sigma_x \\ \sigma_y \\ \tau_{xy} \end{Bmatrix} \tag{4}$$

2.2 Verification of Stress Calculations

To verify the calculation results of ply axis stress in Table 3, the FEA for the hydrogen high pressure vessel (Type 4) designed using netting theory was conducted, and the FEA results were compared with the calculation results for the longitudinal tensile strength (σ_f) and maximum tensile stress (σ_1) of the composite layer in order to assess structure safety. Figure 7 and Table 4 show the FEA results for the helical layer and hoop layer of the composite layer calculated using netting theory (Helical: 6 mm, Hoop: 9.3 mm). The values of the helical layer (11.54°, − 11.54°) and the hoop layer in the cylinder part were calculated to be 1755 Mpa, 1751 MPa, and 2518 MPa, respectively. The errors of the helical layer (inside, outside) and hoop layer were 0.17%, 0.057%, and 0.7%, respectively, so feasibility of the calculation process of the stress of the composite layer using CLT was verified.

3 Design of Composite Layers for a High Pressure Hydrogen Vessel Using the CLT

3.1 Design of Composite Layers in a Cylinder Part

To design a composite layer, for the lamination pattern in which the helical layer (+, −) and the hoop layer (90°, 90°) were repeatedly laminated as shown in Fig. 8, the stress generated in each ply was calculated using Matlab by applying the calculation process shown in Fig. 2.

More specifically, the stress calculation described above was carried out by using Matlab so that output variables can be derived for several input variables, such as burst pressure (P_{burst}), the cylinder radius (r_c), the boss radius (r_o), thickness per ply (t_{ply}), the number of repetition of lamination (b) and the ply number of hoop layer (hn). Also, the coding

Table 2 Calculation of the transformed stiffness and the extensional stiffness

Laminate angle: 11.54°						
Transformed stiffness coefficient (GPa)	$\overline{Q}_{11}$	$\overline{Q}_{12}$	$\overline{Q}_{22}$	$\overline{Q}_{16}$	$\overline{Q}_{26}$	$\overline{Q}_{66}$
	127.2	7.7	9.6	23.5	1.6	9.4
Laminate angle: − 11.54°						
Transformed stiffness coefficient (GPa)	$\overline{Q}_{11}$	$\overline{Q}_{12}$	$\overline{Q}_{22}$	$\overline{Q}_{16}$	$\overline{Q}_{26}$	$\overline{Q}_{66}$
	127.2	7.7	9.6	-23.5	1.6	9.4
Laminate angle: 90°						
Transformed stiffness coefficient (GPa)	$\overline{Q}_{11}$	$\overline{Q}_{12}$	$\overline{Q}_{22}$	$\overline{Q}_{16}$	$\overline{Q}_{26}$	$\overline{Q}_{66}$
	9.1	3.1	137	0	0	4.7
Extensional stiffness coefficient (MN/mm)	A_{11}	A_{12}	A_{22}	A_{16}	A_{26}	A_{66}
	848	75	1332	0	0	100

Table 3 Stress calculation of each plies in composite layer designed by the netting theory

Laminate angle: 11.54°					
ε_x	0.0125	σ_x	1707 MPa	σ_1	1870 MPa
Laminate angle: − 11.54°					
ε_x	0.0125	σ_x	1707 MPa	σ_1	1870 MPa
Laminate angle: 90°					
ε_x	0.0125	σ_x	168.9 MPa	σ_1	2500 MPa

(a) Inside helical layer

(b) Outside helical layer

(c) Hoop layer

Fig. 7 Principal stresses distributions of a composite layer in the cylinder part

was done in such away that when the stress of each ply is higher than the tensile strength of the composite material (2539 MPa), it will be indicated as unsafe, and when it is not, it will be indicated as safe. Regarding the lamination pattern shown in Fig. 8, as the thickness of a composite layer in the cylinder part of Type 4 pressure vessels was minimized, the number of laminations that generates stress lower than the tensile strength of the composite material (2539 MPa) was determined to be 15 times (18 mm) as shown in Table 5, and the stresses in the helical and hoop layers were calculated to be 1203 MPa and 2476 MPa, respectively.

Table 4 Comparison of stress calculation results between CLT and FEA

FEA		CLT		Error
Laminate angle: 11.54 °				
σ_1	1755 MPa	σ_1	1870 MPa	6.2%
Laminate angle: -11.54 °				
σ_1	1751 MPa	σ_1	1870 MPa	6.4%
Laminate angle: 90 °				
σ_1	2518 MPa	σ_1	2500 MPa	1%

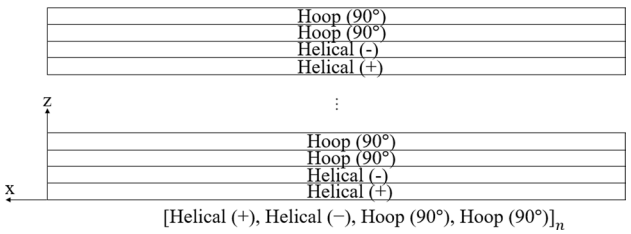

Fig. 8 A lamination pattern of a composite layer (+, −, 90°, 90°)

Table 5 Stress calculation in 15 repeated lamination patterns

Number of ply	15
Total thickness (mm)	18
Helical layer stress (MPa)	1203
Hoop layer stress (MPa)	2476

Table 6 Comparison of stress calculation results using the CLT and the FEA in 15 repeated lamination patterns

	Helical layer	Hoop layer
CLT	1203 MPa	2476 MPa
FEA	1196 MPa	2640 MPa
Error	0.06%	6.1%

In the CLT, it is assumed that when line loads is imposed on the composite layer, the same strain is generated in each ply, and consequently, the stress generated in the hoop layer is calculated to be identical in each ply. In the case of the helical layer, it follows from Eq. (2) that as a ply is closer to the outside, the laminate angle becomes lower and thus stress becomes higher. In consideration of this stress distribution, for the helical layer, the stress of the outside composite layer where stress is relatively higher was presented.

3.2 Verification of Design Results

Table 6 shows the results of the comparison between CLT calculation results and FEA results for the 15-time repeated lamination pattern. The FEA results for the plies where the highest stress is generated (Hoop: inside, Helical: outside) among all plies were compared with CLT calculation results (Hoop layer, Helical layer). As shown in Table 6, for the helical layer, FEA results and CLT calculation results were in good agreement with the error value of 0.06%, but for the hoop layer, there was some disagreement between the stress values of the two data with the error value of 6.1%.

Figure 9 show the FEA results for stresses generated in the innermost and outermost layers of the hoop and helical layers in the cylinder part. In the case of the helical layer, there was almost no difference in stress between the inside layer (1155 MPa) and the outside layer (1196 MPa) with a difference of 3.4%, but in the hoop layer, there was a significant difference in stress (16.9%) between the inside layer (2640 MPa) and the outside layer (2195 MPa). This difference in the stress distribution can be explained as follows. When the internal pressure is applied to the inner wall of the high pressure hydrogen vessel (Type 4), the hoop-direction load generated in the cylinder part is mostly sustained by the hoop layer, and the longitudinal-direction load is mostly supported by a helical layer. As a result, in the helical layer, there is almost no difference in stress depending on the difference in thickness, but in the hoop layer, a ply nearer the outside is subjected to lower stress.

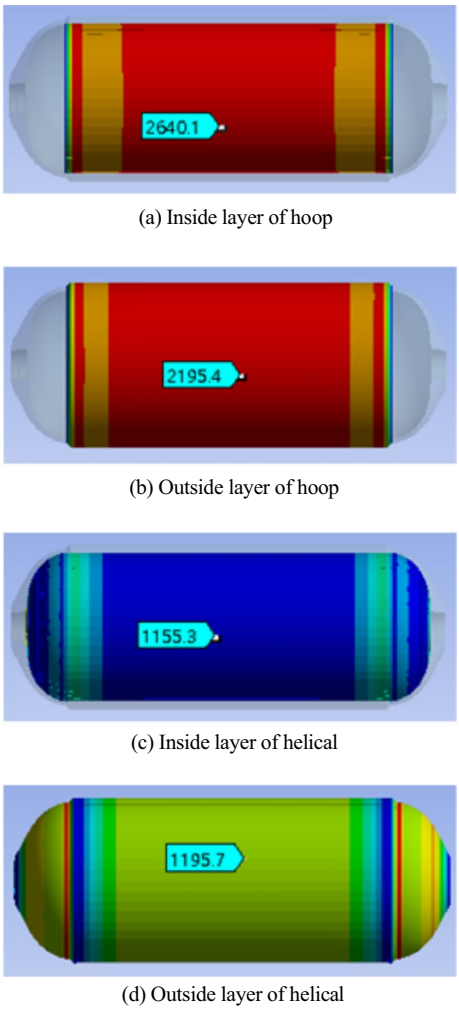

(a) Inside layer of hoop

(b) Outside layer of hoop

(c) Inside layer of helical

(d) Outside layer of helical

Fig. 9 Principal stresses distributions of a composite layer in the cylinder part

3.3 Modified Stress Calculation for Composite Layers in Cylinder Part

In order to deal with the errors between stress calculation results by the CLT and FEA, it is necessary to newly establish the calculation process using CLT. As described above, in the CLT, it is assumed that constant strain is produced in each ply, and as a result, each ply in the hoop layer has the same stress value. Actually, stress generated in the hoop layer is highest in the innermost ply, and the ply nearer the outside has a lower stress value. Figure 10 shows that stress values change depending on the distance from the central axis of the vessel to the composite layer. The stress values of the hoop layer calculated by using the CLT can be considered to actually indicate the stress value at the midpoint position in the laminated composite layer. Therefore, the maximum value (inside layer) and minimum value (outside layer) of stress generated in the hoop layer can be calculated

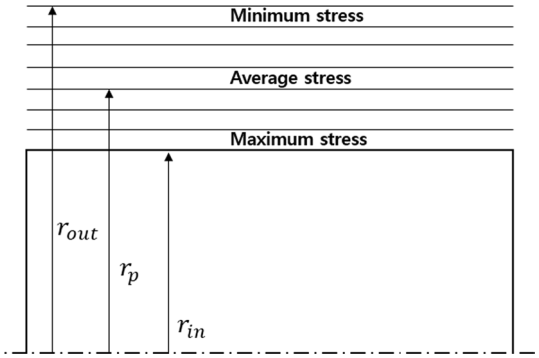

Fig. 10 Maximum and minimum stress of a composite layer according to a distance from the central axis

Table 7 Results of stress calculation using modified the CLT

	Helical layer	Hoop layer
Number of ply (n)	16	
Total thickness (mm)	19.2 mm	
CLT	1131 MPa	2475 MPa
FEA	1105 MPa	2513 MPa
Error	2.3%	1.5%

by using the proportional and inversely proportional relationships of Eqs. (5) ~ (6).

$$r_{in} : r_p = \sigma_p : \sigma_{in} \rightarrow \sigma_{in} = \sigma_p \cdot \frac{r_p}{r_{in}} \tag{5}$$

$$r_{out} : r_p = \sigma_p : \sigma_{out} \rightarrow \sigma_{out} = \sigma_p \cdot \frac{r_p}{r_{out}} \tag{6}$$

The above process was reflected in Matlab coding, and the results of the comparison between the tensile strength of a composite material and the stress value of the hoop layer (inside) are shown in Table 7 and Fig. 11. The total number of repetitions of the lamination pattern was finally determined to be 16 times, and the comparison between the FEA results and CLT calculation results showed that the error value was 2.3% for the helical layer and 1.5% for the hoop layer, so the feasibility of the CLT calculation method described above was confirmed.

Figure 12 shows the FEA results of the stress distribution in the longitudinal direction of the high pressure hydrogen vessel with the composite layer repeatedly laminated 16 times. For the helical layer, the stress distributions of the inside and outside layers where relatively high stress is generated were derived, but for the hoop layer, the stress distribution of the inside layer was represented. Figure 12 shows that while stress values in the longitudinal direction are almost constant in the

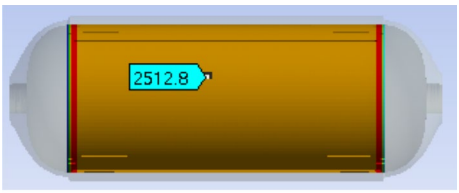

(a) Inside layer of hoop

(b) Outside layer of helical

Fig. 11 Maximum principal stresses of the composite layer generated from 16 repeat pattern

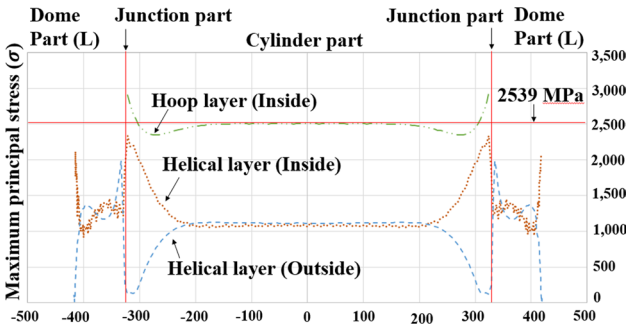

Fig. 12 Maximum principal stresses of hoop and helical composite layers according to z-direction

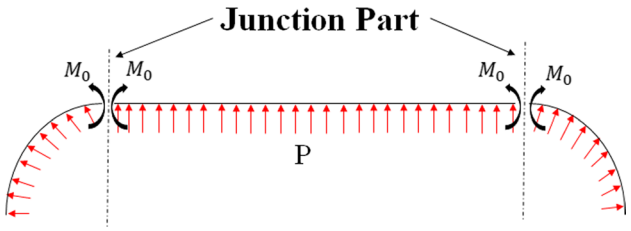

Fig. 13 The line moments generated at junction parts in the high pressure hydrogen vessel (Type 4)

cylinder part, there is a sharp rise in the stress value in the dome part and in the junction part. As shown in Fig. 13, in a pressure vessel, bending stress due to a moment is additionally generated in the junction part due to stress discontinuity between the dome part and the cylinder part [25, 26], and the highest stress is generated in the inside helical layer which receives tensile force compared to the outside ply. This is generally considered the most common cause of the fracture occurred in Type 4 pressure vessels, and fracture actually

occurs in the junction part when burst pressure is applied in fracture testing [18, 27]. Therefore, the theoretical design of the Type 4 pressure vessel requires the calculation of stress due to bending in the junction part.

4 Design of Composite Layers in a High Pressure Hydrogen Vessel Considering Bending Moments

4.1 Design of Composite Layers in a Cylinder Part

When a composite layer is subjected to simultaneous the bending and stretching, the stress thereby generated can be calculated by adding the two results as shown in Eq. (7)

$$\begin{Bmatrix} \sigma_x \\ \sigma_y \\ \tau_{xy} \end{Bmatrix} = \left[\overline{Q}_{ij}\right] \begin{Bmatrix} \varepsilon_x^o \\ \varepsilon_y^o \\ \gamma_{xy}^o \end{Bmatrix} + z\left[\overline{Q}_{ij}\right] \begin{Bmatrix} k_x \\ k_y \\ k_{xy} \end{Bmatrix} \tag{7}$$

The left term of the right-hand side of Eq. (7) can be obtained through the calculation processes of Fig. 3 explained earlier, and to calculate the right term, a curvature (k) of the composite layer needs to be calculated. The line moment occurring in the composite layer can be determined by multiplying the curvature (k) by the bending stiffness as shown in Eq. (8), and the bending stiffness matrix ($D_{\alpha\beta}$) is defined by Eq. (9). In Eq. (9), z_{ku} is the distance from the midpoint of the total thickness of a composite layer to the top surface of the n^{th} ply, and z_{kl} is the distance from the midpoint of the total thickness of a composite layer to the bottom surface of the n^{th} ply, as shown in Fig. 14.

$$\begin{Bmatrix} M_x \\ M_y \\ M_{xy} \end{Bmatrix} = \left[D_{\alpha\beta}\right] \begin{Bmatrix} k_x \\ k_y \\ k_{xy} \end{Bmatrix} \tag{8}$$

$$D_{\alpha\beta} = \sum_{k=1}^{n} \overline{Q}_{ij} \left(\frac{z_{ku}^3 - z_{kl}^3}{3} \right) \tag{9}$$

Therefore, the curvature (k) by the bending moment is defined by Eq. (10). In Eq. (10), $d_{\alpha\beta}$ is the inverse of bending stiffness ($D_{\alpha\beta}$).

$$\begin{Bmatrix} k_x \\ k_y \\ k_{xy} \end{Bmatrix} = \begin{bmatrix} d_{11} & d_{12} & d_{16} \\ d_{12} & d_{22} & d_{26} \\ d_{16} & d_{26} & d_{66} \end{bmatrix} \begin{Bmatrix} M_x \\ M_y \\ M_{xy} \end{Bmatrix} \tag{10}$$

If the curvature (k) is obtained by Eq. (10), the stress by bending of the nth ply can be determined by Eq. (11), and finally, ply axis stress due to bending is calculated by Eq. (4) explained earlier.

$$\begin{Bmatrix} \sigma_x \\ \sigma_y \\ \sigma_z \end{Bmatrix}^n = z^k \left[\overline{Q}_{ij}\right] \begin{Bmatrix} k_x \\ k_y \\ k_{xy} \end{Bmatrix} \tag{11}$$

4.2 Design of Composite Layers in a Cylinder Part

To calculate the bending stress mentioned above, a curvature (k) needs to be determined by Eq. (10), and to calculate the curvature (k), it is necessary to determine the value of the line moment (M_0) acting on the junction part of the composite layer when internal pressure is applied to the high pressure hydrogen vessel as shown in Fig. 13. The moment acting on the junction part is generated by the internal pressure applied to the dome part, and in the case of the pressure distribution of the dome part, the load is divided in the x and z directions. In both directions, the cross-sectional area continuously changes in the longitudinal direction, and both ends are constrained by the boss part and the cylinder part, so the dome part can be assumed as a beam under a linear distribution load, as shown in Fig. 15. The moments (M_x, M_z) of the beam supported at both ends under the linear distribution load shown in Fig. 15 can be obtained by a fourth-order differential equation. The linear distributed load (q) of the beam supported at both ends can be expressed by Eq. (12) and

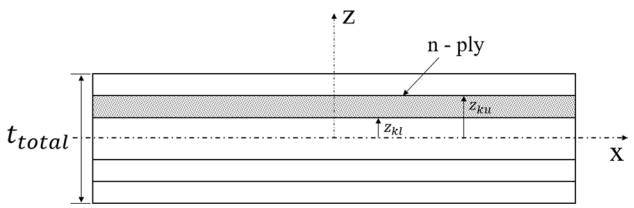

Fig. 14 Definitions of z_{ku} and z_{kl} in composite layers

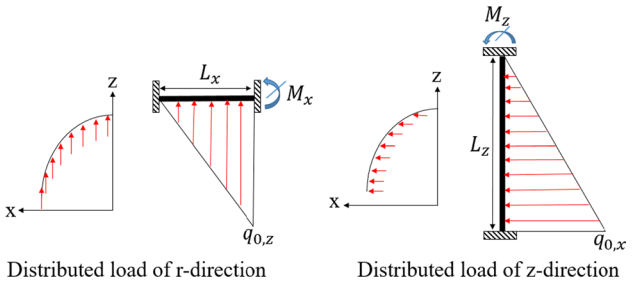

Fig. 15 Linear distributed loads of support beams at both ends

the differential equation is expressed by Eq. (13). Where, q_0 is maximum intensity of the linear distributed load.

$$q = q_0 \frac{x}{L} \tag{12}$$

$$EI\frac{d^4v}{dx^4} = -q = q_0 \frac{x}{L} \tag{13}$$

The shear force V and the moment M are derived from the relationship with the intensity q of the linear distributed load, and they are defined by Eqs. (14) and (15), respectively. Where, $C_1 \sim C_2$ are integration constants. Therefore, the moments of the beam supported at both ends is calculated by Eqs. (16) ~ (17).

$$EI\frac{d^3v}{dx^3} = -q_0 \frac{x^2}{2L} + C_1 \tag{14}$$

$$EI\frac{d^2v}{dx^2} = M = -q_0 \frac{x^3}{6L} + C_1 x + C_2 \tag{15}$$

$$M_z = -\frac{q_{0,x} L_z^2}{30} [\text{N mm}] \tag{16}$$

where $q_{0,x}$ is x-direction maximum intensity, L_z is z-direction length of the dome part under the linear distributed load.

$$M_x = \frac{q_{0,z} L_x^2}{20} [\text{N mm}] \tag{17}$$

where $q_{0,z}$ is x-direction maximum intensity, L_x is z-direction length of the dome part under the linear distributed load.

Equations (18) ~ (19) were obtained by dividing Eqs. (16) ~ (17) into circumference ($2 \cdot \pi \cdot r_A$). Where, $M_{z,L}$ and $M_{x,L}$ are the line moments for the distributed load applying in the x-direction and the z-direction, respectively.

$$M_{z,L} = -\frac{q_{0,x} L_z^2}{60 \cdot \pi \cdot r_A} [\text{N mm/mm}] \tag{18}$$

$$M_{x,L} = \frac{q_{0,z} L_{xz}^2}{40 \cdot \pi \cdot r_A} [\text{N mm/mm}] \tag{19}$$

To calculate the line moments ($M_{z,L}$, $M_{x,L}$) in the junction part by Eqs. (18) ~ (19), it is necessary to determine the value of q_0. The value of q_0 was obtained by multiplying the circumference of the pressure vessel at the point where occurs by burst pressure ($P_{burst} = 157.5$ MPa) as shown in Eqs. (20) ~ (21). Where, $r_{c,inner}$ is the cylinder inner radius, r_x is the maximum median radius of dome part as shown in Fig. 16.

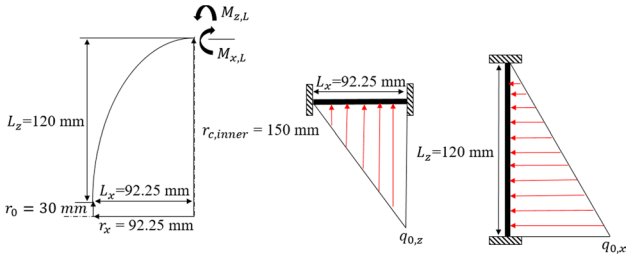

Fig. 16 The line moments ($M_{x,L}$, $M_{z,L}$) occurred in the junction part of the high pressure hydrogen pressure vessel (Type 4)

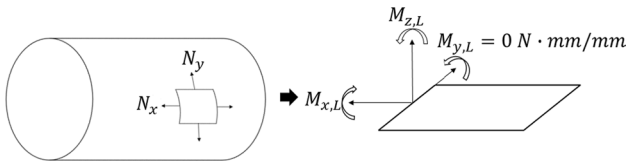

Fig. 17 The line moments generated at the junction part when the cylinder part unfolded

$$q_{0,x} = 2 \cdot \pi \cdot r_x \cdot P_{burst} \tag{20}$$

$$q_{0,z} = 2 \cdot \pi \cdot r_{c,inner} \cdot P_{burst} \tag{21}$$

Equations (18) ~ (19) can be rewritten as Eq. (22) ~ Eq. (23) by substituting Eqs. (20) ~ (21) into Eqs. (18) ~ (19), and they were reflected in the curvature calculation formula of Eq. (10). Where, r_A is the distance from the central axis to the midpoint of the total thickness of the laminated composite layer.

$$M_{z,L} = -\frac{P_{burst} \cdot L_z^2 \cdot r_x}{30 \cdot r_A} [\text{N mm/mm}] \tag{22}$$

$$M_{x,L} = \frac{P_{burst} \cdot L_x^2 \cdot r_{c,inner}}{20 \cdot r_A} [\text{N mm/mm}] \tag{23}$$

Figure 17 shows the line moments acting on the unfolded plane of the cylinder part. The occurrence of bending stress in the hoop layer requires the generation of moment in the y-direction, but in a pressure vessel, the moment in the y-direction does not occur when internal pressure is applied. However, as shown in Fig. 12, it can be seen that as the stress value was increased even at both ends of the hoop layers, stress higher than tensile strength (2539 MPa) was generated. Figure 18 shows the deformation of the junction part induced by the x-axis line moment ($M_{x,L}$). The x-axis line moment ($M_{x,L}$) causes deflection in the helical layer, which results in a change in diameter

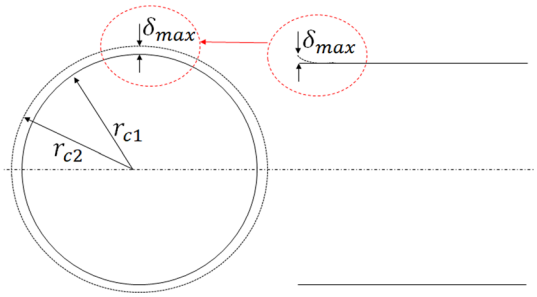

Fig. 18 Deformation of the junction part by the x-axis line moment in the high pressure hydrogen vessel (Type 4)

Fig. 19 Maximum deflection in a beam supported at both ends

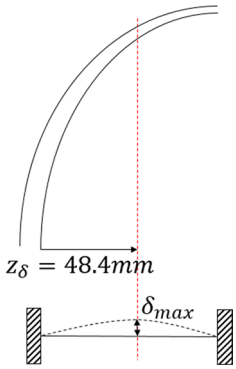

of the hoop layer, and this difference in the diameter increases the stress of the hoop layer in the junction part.

The maximum deflection of a beam supported at both ends under a linear distribution load occurs at the point where the slope is 0 as shown in Fig. 19, and the maximum deflection can be rewritten as Eq. (25) by Eq. (24). In this case, the point where the maximum deflection occurs was determined to be $z_\delta = 48.4$ mm by Eq. (26).

$$EIv = -q_0\frac{x^5}{120L} + C_1\frac{x^3}{6} + C_2\frac{x^2}{2} + C_3x + C_4 \tag{24}$$

$$\delta_{max} = -\frac{q_{0,z}}{120EI}\left(\frac{z_\delta^5}{L_x} - 3\cdot L\cdot z_\delta^3 + 2\cdot L^2\cdot xz_\delta^2\right) \tag{25}$$

$$z_\delta = \frac{L\left(\sqrt{105}-5\right)}{10} \tag{26}$$

If the maximum deflection in a beam supported at both ends is determined, strain can be calculated by using the circumference of a junction part obtained through the diameter difference as shown in Eq. (27). Finally, stress due to deflection can be calculated by multiplying strain by the stiffness coefficient in the fiber direction, as shown in Eq. (28).

Table 8 Stress calculation considering a bending moment in 16 repeated lamination patterns

	Helical layer stress	Hoop layer stress
Number of ply	16	
Total thickness	19.2 mm	
CLT	2330 MPa	2803 MPa
FEA	2163 MPa	2775 MPa
Error	7.2%	1%

(a) Inside layer of helical

(b) Outside layer of hoop

Fig. 20 Maximum principal stresses of the composite layer considering bending moment generated from 16 repeat pattern

$$\varepsilon_{hoop} = \frac{2\pi r_{c2} - 2\pi r_{c1}}{2\pi r_{c1}} \tag{27}$$

$$\sigma_{hoop} = E_1 \times \varepsilon_{hoop} \tag{28}$$

The calculation process of bending stress in the composite layer described above was added to Matlab, and the results were added together with the stress calculation results derived by stretching. Table 8 and Fig. 20 shows the calculation results of stress occurring in the junction part of the composite layer obtained by considering bending stress for the 16-time repeated lamination pattern, and these calculation results were compared with FEA results. The errors between the CLT and the FEA results were 6.7% in the helical layer (2318 MPa, 2163 MPa) and 1% in the hoop layer (2803 MPa, 2775 MPa), so the feasibility of the CLT method was verified.

4.3 Ply Axis Stress Calculation Results

Based on the CLT method for the high pressure hydrogen vessel (Type 4) derived in this study, the pattern design of

a composite layer was conducted. Laminations were performed in the order of the helical layer (+, −) and the hoop layer (90°, 90°). Stress calculation of a composite layer was carried out as shown in Fig. 21, increasing the number of repeated pattern plies, which is satisfied with structural safety, compared stress of the composite layer with its tensile strength (2539 MPa). As the thickness of the composite layer in the junction part was minimized, the number of laminations that generates stress lower than the tensile strength (2539 MPa) was determined to be 18 times as shown Table 9. The stress calculation results were compared with FEA results of Fig. 22, and its result showed that the error values in the helical and hoop layers were 0.9% and 3.4%, respectively.

5 Conclusion

In the present study, the method to calculate the stress generated in each ply of composite layers was developed by applying the CLT to the design of the high pressure hydrogen vessel (Type 4). The developed CLT design method described above was compared with the FEA results to evaluate the feasibility of the design method using CLT and its results are summarized as follows.

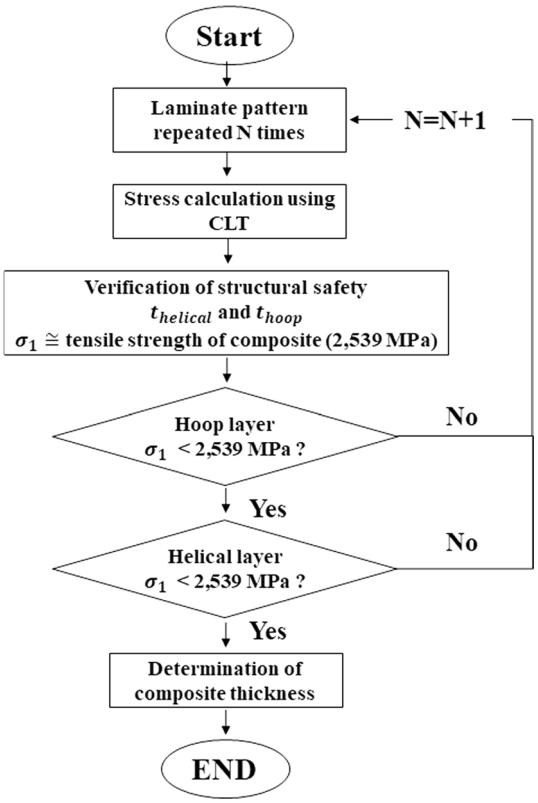

Fig. 21 Flow chart for design of a composite layer using the CLT

Table 9 Stress calculation considering a bending moment in 18 repeated lamination patterns

	Helical layer stress	Hoop layer stress
Number of ply	18	
Total thickness	21.6 mm	
CLT	1940 MPa	2454 MPa
FEA	1943 MPa	2541 MPa
Error	0.2%	3.4%

1. Based on the developed CLT method, this study also performed the design of the thickness and a pattern of the composite layer of the high pressure hydrogen vessel (Type 4) that can satisfy weight reduction.
2. The method of composite layer design using the CLT was possible the calculation of stress in the junction part by applying the line load ($N_{x,L}$, $N_{y,L}$) and the line moment and can embody real repeated pattern of the composite layer.
3. As the thickness of composite layer in the junction part was minimized, the number of laminations that generates stress lower than the tensile strength (2539 MPa) was determined to be 18 times.
4. The errors between the FEA and the CLT were 0.9% in the helical layer and 3.4% in the hoop layer, so the feasibility of the stress calculation method using CLT was confirmed.
5. Because the CLT design method to develop in the study can calculate stress of the junction part and embody real repeated pattern of the composite layer, it is considered for the CLT design method to be possible in near optimal

(a) Inside layer of helical

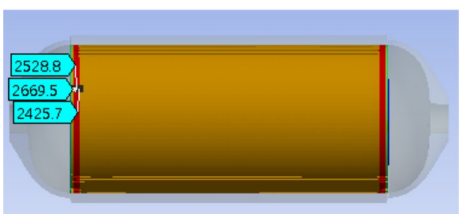

(b) Outside layer of hoop

Fig. 22 Maximum principal stresses of the composite layer considering bending moment generated from 16 repeat pattern

design with more accuracy than the netting theory and with more rapid than FEA.

Acknowledgements This work was supported by Materials/Parts Technology Development Program (No. 20015893) funded By the Ministry of Trade, industry & Energy(MI, Korea).

Author contributions Both authors read and approved the final manuscript.

Competing interest The authors declare no competing financial interests.

References

1. Nonobe, Y. (2017). Development of the fuel cell vehicle mirai. *IEEJ Transactions of Electrical and Electronic Engineering, 12*(1), 5–9.
2. Panwar, N. L., Kaushik, S. C., & Kothari, S. (2011). Role of renewable energy sources in environmental protection: A review. *Renewable and Sustainable Energy Reviews, 15*(3), 1513–1524.
3. Ball, M., & Weeda, M. (2015). The hydrogen economy-vision or reality? *Compendium of Hydrogen Energy, 40*(25), 7903–7919.
4. Kim, K., & Kwon, T. K. (2020). Characteristics of temperature-pressure of metal-hydride actuation system using hydrogen pressure change. *International journal of Precision Engineering and Manufacturing, 21*(9), 1763–1770.
5. Kim, M. S., Lee, J. H., & Kwak, M. K. (2020). Review : Surface texturing methods for solar cell efficiency enhancement. *International Journal of Precision Engineering and Manufacturing, 21*(7), 1389–1398.
6. Rahim, A., Tijani, A., Mohamed, W., Hanapi, S., & Sainan, K. (2015). An overview of hydrogen production from renewable energy soruce for remote area application. *Applied Mechanics and Materials, 699*, 474–479.
7. John, J., Kast, J., Morrison, G., & Marcinkoski, J. (2017). Design space assessment of hydrogen storage onboard medium and heavy duty fuel cell electric trucks. *Journal of Electrochemical Energy Conversion and Storage, 14*(2), 021004.
8. Li, W., Ye, J., Cui, Y., Kim, N., Cha, S. W., & Zheng, C. (2022). A speed reinforcement learning-based energy management strategy for fuel cell hybrid vehicles considering fuel cell system lifetime. *International Journal of Precision Engineering and Manufacturing-Green Technology, 9*(5), 859–872.
9. Lv, H., Shen, G., Yu, Y., Zhu, L., & Zhou, R. (2021). Defect detection in the winding layer of CNG composite-wound Cylindersvrture of minimal mechanism is that it allows. *International Journal of Precision Engineering and Manufacturing, 22*(12), 1937–1946.
10. Zheng, C., Li, W., Li, W., Xu, K., Peng, L., & Cha, S. W. (2022). A deep reinforcement learning-based energy management strategy for fuel cell hybrid buses. *International Journal of Precision Engineering and Manufacturing-Green Technology, 9*(5), 885–897.
11. Barthelemy, H., Weber, M., & Barbier, F. (2017). Hydrogen storage : Recent improvements and industrial perspectives. *International Journal of Hydrogen Energy, 42*(11), 7254–7262.
12. Humberto, J., Almeida, S., Faria, H., Marques, T., & Amico, C. (2014). Load sharing ability of the liner in type III composite pressure vessels under internal pressure. *Journal of Reinforced Plastics & Composites, 33*(24), 2274–2286.
13. Musthak, M. D., Madar, P., & Narayana, S. (2016). Prediction of transverse directional strains and stresses of filament wound composite pressure vessel by using higher order shear deformation theories. *International Journal of Composite Materials, 6*(3), 79–87.
14. Cho, S. M., Kim, K. S., Lee, S. K., Jung, G. S., Lee, S. K., & Lyu, S. K. (2018). Effect of dome curvature on failure mode of type 4 composite pressure vessel. *International Journal of Precision Engineering and Manufacturing, 19*(3), 405–410.
15. Sapre, S., Pareek, K., & Vyas, M. (2020). Investigation of structural stability of type IV compressed hydrogen storage tank during refueling of fuel cell vehicle. *Journal of Energy Storage, 2*(4), e150.
16. Alcantar, V., Aceves, S. M., Ledesma, E., Ledesma, E., Ledesma, S., & Aguilera, E. (2017). Optimization of Type 4 composite pressure vessels using genetic algorithms and simulated annealing. *International Journal of Hydrogen Energy, 42*(24), 15770–15781.
17. Hua, T. Q., Roh, H. S., & Ahluwalia, R. K. (2017). Performance assessment of 700-bar compressed hydrogen storage for light duty fuel cell vehicles. *International Journal of Hydrogen Energy, 42*(40), 25121–25129.
18. Leh, D., Saffre, P., Francescato, P., Arrieux, R., & Villalonga, S. (2015). A progressive failure analysis of a 700-bar type IV hydrogen composite pressure vessel. *International Journal of Hydrogen Energy, 40*(38), 13206–13214.
19. Jois, K. C., Welsh, M., Gries, T., & Sackmann, J. (2021). Numerical analysis of filament wound cylindrical composite pressure vessels accounting for variable dome contour. *Journal of Composites Science, 5*(2), 56–71.
20. Zhang, Q., Xu, H., Jia, X., Zu, L., Cheng, S., & Wang, H. (2020). Design of a 70 MPa type IV hydrogen storage vessel using accurate modeling techniques for dome thickness prediction. *Composite Structures, 236*(3), 111915–111925.
21. Xia, M., Takayanagi, H., & Kemmochi, K. (2001). Analysis of multi-layered filament wound composite pipes under internal pressure. *Composite Structures, 53*(4), 483–491.
22. Cetin, M., & Yaman, K. (2020). Location size and orientation effect of semi-elliptical surface crack on the fracture of a type-3 composite pressure vessel using J-integral method. *Defence Science Journal, 70*(1), 23–34.
23. Parnas, L., & Katirci, N. (2002). Design of fiber-reinforced composite pressure vessels under various loading conditions. *Composite Structures, 58*(1), 83–95.
24. Park, G. Y., Jang, H. S., & Kim, C. (2021). Design of composite layer and liner for structure safety of hydrogen pressure vessel (type 4). *Journal of Mechanical Science and Technology, 35*(8), 3507–3517.
25. Solazzi, L., & Vaccari, M. (2022). Reliability design of a pressure vessel made of composite materials. *Composite Structures, 279*(1), 114726–114737.
26. Daghia, F., Baranger, E., Tran, D. T., & Pichon, P. (2020). A hierarchy of models for the design of composite pressure vessels. *Composite Structures, 235*(1), 111809–111827.
27. Son, D. S., & Chang, S. H. (2021). Evaluation of modeling techniques for a type III hydrogen pressure vessel (70 MPa) made of an aluminum liner and a thick carbon/epoxy composite for fuel cell vehicles. *International Journal of Hydrogen Energy, 37*(3), 2353–2369.

Gunyoung Park received Ph.D. degrees in school of Mechanical Engineering, Pusan National Univrsity, South Korea, in 2022. His major research fields are Design of Type 4 high pressure hydrogen vessel, element finite analysis and metal forming.

Chul Kim received M.S. and Ph.D. degrees in 1987 and 1994. Professor Kim is currently a Professor at the Research Institute of Mechanical Technology of Pusan National University in Busan. His research fields include FEM simulation (structures, dynamics, and fluid analysis), optimal structural design, and CAD/CAM.